RESEARCH ARTICLE

NANOPHOTONICS

Wafer-scale δ waveguides for integrated two-dimensional photonics

Myungjae Lee^{1,2}†, Hanyu Hong³†, Jaehyung Yu³, Fauzia Mujid³, Andrew Ye⁴, Ce Liang⁴, Jiwoong Park^{1,3,4}*

The efficient, large-scale generation and control of photonic modes guided by van der Waals materials remains as a challenge despite their potential for on-chip photonic circuitry. We report three-atom-thick waveguides— δ waveguides—based on wafer-scale molybdenum disulfide (MoS $_2$) monolayers that can guide visible and near-infrared light over millimeter-scale distances with low loss and an efficient in-coupling. The extreme thinness provides a light-trapping mechanism analogous to a δ -potential well in quantum mechanics and enables the guided waves that are essentially a plane wave freely propagating along the in-plane, but confined along the out-of-plane, direction of the waveguide. We further demonstrate key functionalities essential for two-dimensional photonics, including refraction, focusing, grating, interconnection, and intensity modulation, by integrating thin-film optical components with δ waveguides using microfabricated dielectric, metal, or patterned MoS $_2$.

hin-film waveguides that can confine, direct, and modulate light waves on-chip are key ingredients in modern photonic technologies (1-6). However, because the optical fields are located inside of the waveguides, the integration of multiple photonic components made of distinct materials requires careful tuning of each component's dimensions (characteristic size d), which are customized for individual operation wavelengths (λ) and the specific optical properties of the materials used (refractive index n) to keep the ratio nd/λ similar (typically of the order of unity) throughout the device (1-11). One fundamental challenge in integrated photonics is to develop an architecture that enables efficient waveguiding and interconnection free of such spectral and materials constraintsa challenging goal for waveguides with fixed dimensions.

δ Waveguides: Principle and operation

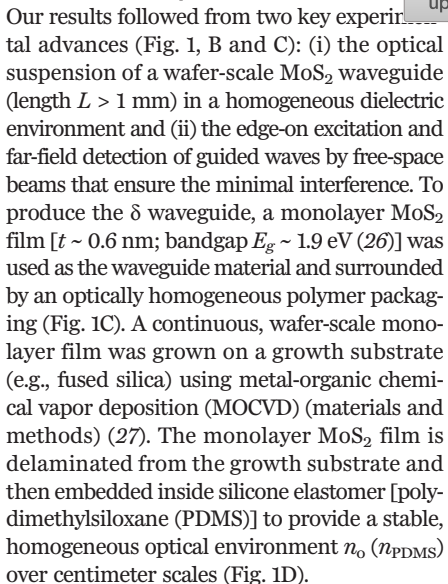
A conceptual approach is a δ waveguide, whose ultrasmall thickness t satisfying $nt/\lambda \ll 1$ enables broadband, single-mode operation, where the out-of-plane confinement of a guided mode and its in-plane propagation can be independently controlled. This type of waveguide has a unique analytic solution when $n > n_0$ (where n_0 is the refractive index of the surrounding medium). The transverse electric (TE) field

¹James Franck Institute, University of Chicago, Chicago, IL 60637, USA. ²Department of Materials Science and Engineering, Seoul National University, Seoul 08826, South Korea. ³Department of Chemistry, University of Chicago, Chicago, IL 60637, USA. ⁴Pritzker School of Molecular Engineering, University of Chicago, Chicago, IL 60637, USA. *Corresponding author. Email: jwpark@uchicago.edu †These authors contributed equally to this work.

profile along the confining z direction $[E_y(z)]$ (Fig. 1A) is an optical analog of a quantum mechanical eigenfunction for a one-dimensional (1D) δ -potential trap. In particular, the imaginary wave vector along the z direction $|k_z|$ is much smaller than $k_{\parallel}=(k_x^2+k_y^2)^{1/2}$ regardless of n or λ (see supplementary text, section S1, for details). Because most of the optical fields are located outside of the waveguide owing to the thinness, this results in an effective mode index $n_{\rm eff}\approx n_0$ and a phase velocity $v\approx v_0=c/n_0$ (where c is the speed of light). The guided mode is therefore described by $\omega=v\times k_{\parallel}$, which is the dispersion relation of a plane wave confined in 2D space.

van der Waals (vdW) materials, such as graphene and monolayer transition metal dichalcogenides (TMDs), provide an ultrathin platform that is ideal for a δ waveguide. For example, long-range propagation of guided waves was predicted in TMDs when the TMD is surrounded by identical optical environments (above and below) (12). However, efficient largescale generation and control of photonic modes guided by vdW materials remains a challenge; although vdW materials have been used as waveguides in recent studies of surface polaritons (13-20) or exciton-polariton waves (21-25), their mechanisms of waveguiding are limited by unsuitable geometry for integration and short propagation lengths. Realizing the full potential of δ waveguides would require the careful implementation of several capabilities, including a large-scale, high-quality vdW film in optically homogeneous medium, systematic coupling and detection mechanisms with minimal interference to the guided wave propagation, and a means to manipulate the guided wave using integrated components.

Fabrication and experimental results

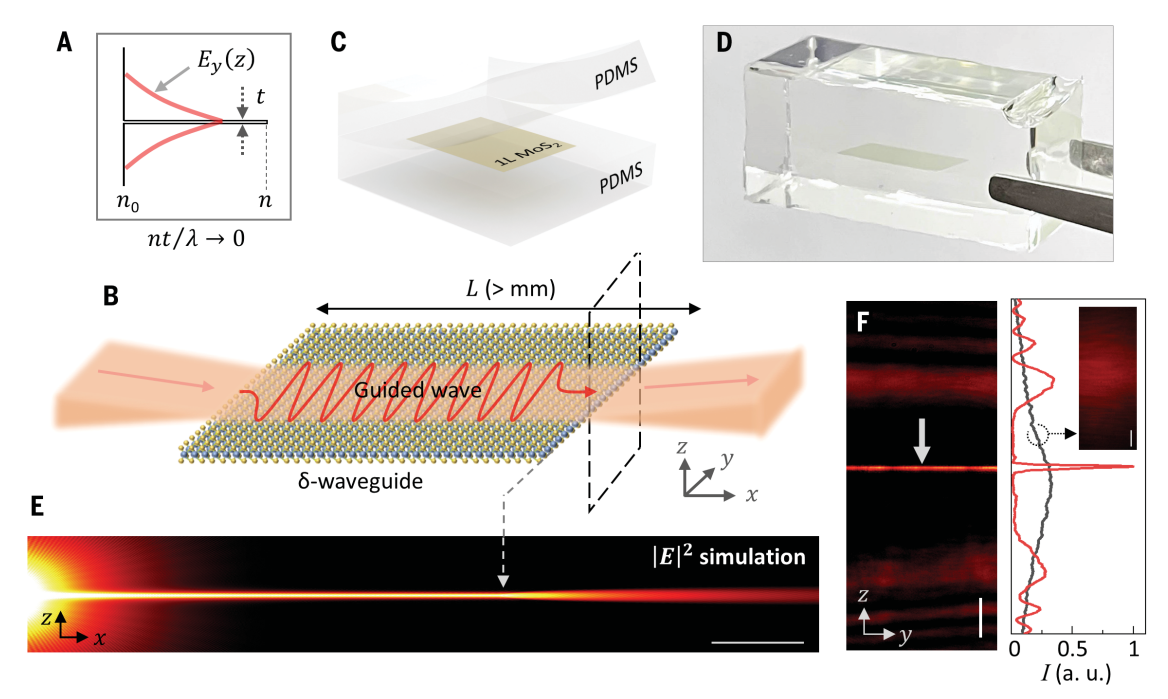


For an efficient excitation, we use electrodynamic simulations to design an optimal geometry for the incident laser beam. Figure 1E shows a calculated distribution of electric field intensity $|E(x, z)|^2$ (materials and methods) when a light wave propagates (from left to right) along a monolayer MoS2 (mode width is approximately a few micrometers) and out-couples into free space at its end (Fig. 1E, dashed arrow). This explains how a guided wave in the δ waveguide couples with a free beam for its excitation and launching. In our experiments, a color-controlled (from 500 to 900 nm), slightly converging laser beam [numerical aperture (NA) ~ 0.1; focused beam width ~ $6 \mu m$] is introduced at the edge of the MoS₂, with the beam center trajectory parallel to the MoS₂ surface (tilting angle $\theta \sim 0$). For detection, the end-face microscopy measures the cross-sectional intensity profile at the end of the MoS₂ waveguide (Fig. 1B, dashed box), and the dark-field microscopy measures the optical fields distribution on MoS2 film by collecting elastically scattered light from the waveguide surface (materials and methods).

Figure 1F (left) displays representative beam profiles measured in end-face imaging with (main panel) and without (inset) a monolayer MoS_2 waveguide ($L \sim 4$ mm) placed in the beam path (λ = 720 nm). The comparison reveals an intense out-coupled light field at the waveguide plane (arrow) that is observed only when the MoS₂ is present. The transverse line profile (right) confirms that the light field at the end of the MoS2 is much stronger than the field outside the waveguide (red line) or that of the laser beam without the waveguide (gray). The intense light field is vertically confined (width ~ 3 µm) and detected only with TE polarized excitation. From the two profiles, we measure that 15% of the total incident beam energy out-couples from the waveguide. After considering

Fig. 1. Large-scale δ waveguides realized by monolayer MoS₂.

(A) Schematic of a transverse profile of a light field trapped by an ultrathin waveguide. (B) Experimental schematic for the excitation and detection of a guided wave. A slightly converging laser beam is injected to the edge of the film with a beam trajectory nearly parallel to the film. These guided waves are observed through filmsurface and end-face imaging microscopy. (C) Schematic of an optically suspended ultrathin film surrounded by optically homogeneous polymer packaging. (D) Photograph of a large-scale δ waveguide obtained by the optical suspension of a monolayer



MoS₂ film. The size of the MoS₂ waveguide is $\sim 0.5 \times 2$ cm². (**F**) Simulated electric field intensity when a light wave propagates along a waveguide and out-couples into free space at the end face of MoS₂ (arrow), calculated for a monolayer MoS₂. Scale bar, 20 μ m. (**F**) Experimentally measured end-face image of δ waveguide with focus at the dashed box shown in (B) upon edge-on incidence of an excitation laser beam with a tailored wavefront (left), and corresponding line profiles measured with (red curve) and without (black curve) the waveguide (right). The inset shows the end-face imaging without the waveguide. Scale bars, 100 μ m. a.u., arbitrary units.

the measured propagation power loss of ~3 dB (fig. S1), we estimate that the in-coupling efficiency is ~30%. Figure 2A further shows a topview image measured from the MoS_2 plane under similar conditions (λ = 720 nm; TE polarization). The image clearly shows strong signals from the MoS_2 surface along the laser path (i.e., the x axis) having a lateral width similar to the beam diameter (~100 μ m).

Figure 2B presents an array of top-view images $[I_{DF}(x, y)]$; like Fig. 2A] collected for $\lambda =$ $500 \sim 900 \text{ nm} (\Delta \lambda = 20 \text{ nm}) \text{ from a centimeter-}$ long monolayer (1L) MoS2 waveguide. For longer $\lambda > 700$ nm, the line remains intense over the entire image (length > 6 mm), whereas for shorter λ , it only maintains signal for a couple of millimeters or less. These dark-field signals are detected only with a TE-mode laser and completely disappear for transverse magnetic (TM) polarization (fig. S2), consistent with the prediction based on excitonic responses of MoS_2 film (12). For N dependence (where N is the layer number), similar dark-field images are shown for a trilayered (3L) MoS2 waveguide (Fig. 2C), which is fabricated by stacking two additional MoS2 monolayers on top of a monolayer MoS_2 waveguide (28). At all λ , the signal decays faster in the 3L waveguide. Similarly, fast decays are observed from a bilayer (2L) MoS₂ waveguide (fig. S3). Figure 2D shows the rate of dark-field signal decay $\beta = 2 \times Im$ (k_x)] in monolayer MoS₂ waveguide (empty circles) as a function of λ , measured from the slopes of $I_{DF}(\propto e^{-\beta x})$ in log scale (fig. S4A). The $\beta(\lambda)$ plot closely matches the expected loss (green curve) calculated on the basis of the absorption spectrum of a monolayer MoS₂ (fig. S4, B and C). For photon energies below $E_{\rm g}$, where the MoS₂ absorption is small, the propagation loss is small ($\beta \sim 0.5$ dB/mm). A similar analysis conducted for different N at $\lambda = 550$ nm suggests that the decay rate substantially increases for thicker waveguides (Fig. 2E).

The guided wave is stable only under a highly symmetric optical environment ($\Delta n \sim 0$), which can be quantitatively described using a direct analogy with a quantum mechanical eigenfunction in a δ-potential well, as illustrated in Fig. 2F. When the vacuum level of a δ -potential trap is asymmetric (ΔV), the confinement becomes weaker on the side with the lower barrier height, and there no longer exists a trapped eigenstate when $\Delta V > 2m\alpha^2/\hbar^2$ (where α is the δ -potential strength, m is the mass of the trapped particle, and \hbar is the reduced Planck constant). We experimentally test this prediction by introducing a liquid environment with tunable refractive index; a monolayer MoS2 film grown on a fused silica substrate ($n_{\rm FS}$) is placed inside an optical cube filled with a water-glycerol solution (n_{mix} ; see Fig. 2G). We vary $\Delta n = n_{\rm mix} - n_{\rm FS}$ by changing the solution composition and measure the guided mode intensity from monolayer MoS₂ $(\lambda = 750 \text{ nm})$. The results shown in Fig. 2H are fully consistent with our analytic predictions (fig. S4D). For $\Delta n/n_{\rm o} < 0.1\%$, the strong signals are visible over the entire field of view (>3 mm). At higher $\Delta n/n_{\rm o} \ge 0.2\%$, the signals are substantially weaker, disappearing completely at 0.9% (see supplementary text, section S3, for more quantitative analysis). Further analysis using a highly collimated laser confirms that $n_{\rm eff} \sim n_{\rm o}$ and $k_z/k_\parallel < 10^{-3}$ and thus that the guided waves are in a form of 2D light waves having negligible out-of-plane dispersion (fig. S5).

These results on the polarization-, wavelength-, layer number N-, and Δn -dependent properties confirm that a MoS $_2$ monolayer can be used to generate a large-scale δ waveguide with propagation loss as low as ~0.5 dB/mm for a broad range of λ and a high (~30%) coupling efficiency. The propagation loss and coupling efficiency could be further improved by material improvement [e.g., optical quality of PDMS and fused silica or reduction of midgap loss in MoS $_2$ (29)] and mode optimization of the excitation laser.

A platform for 2D photonics

The guided mode in a δ waveguide is essentially an evanescent wave whose optical fields are found mostly outside the waveguide (>98%; fig. S6). Engineering optical properties of the surrounding will directly tune the mode index ($n_{\rm eff} \approx n_{\rm o}$) and would change the propagation properties of the guided modes. In addition, the monolayer MoS₂ waveguide can be grown, delaminated, and transferred in large multiinch scale, with both bottom and top surfaces

Lee et al., Science 381, 648-653 (2023) 11 August 2023 2 of 6

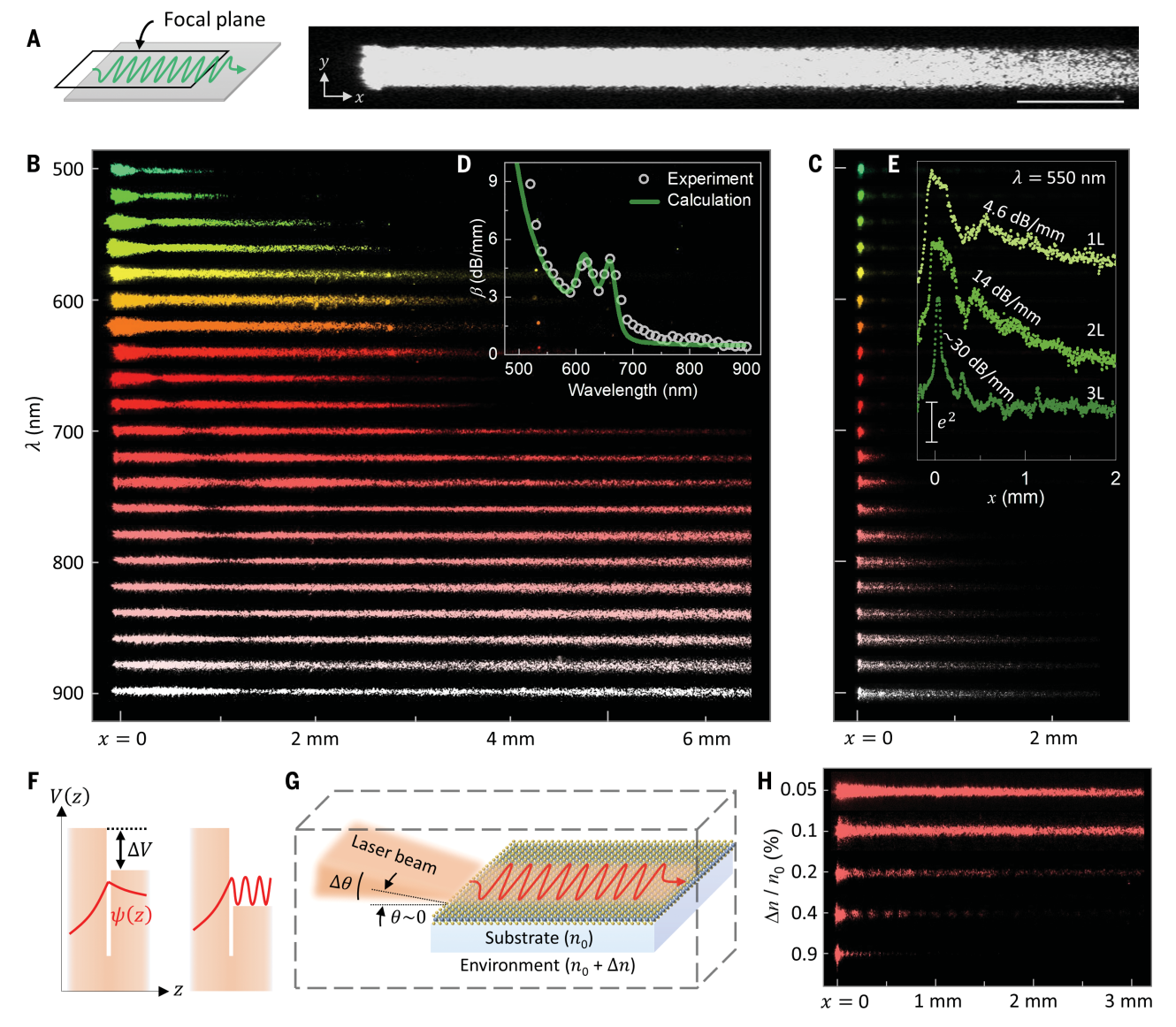


Fig. 2. Light modes guided by & waveguides. (**A**) Film-surface microscopy image on a MoS_2 film, visualized by collecting dark-field signals at λ = 720 nm. Scale bar, 0.2 mm. (**B** and **C**) False-color dark-field images measured from monolayer (B) and 3L (C) MoS_2 waveguides excited at different λ (from 500 to 900 nm). (**D**) Rate of dark-field signal decays as a function of light wavelength (white dots), analyzed from intensity profiles shown in (B), by taking an average slope. The green curve plots the propagation loss of guided waves calculated independently by using the experimental values of sheet susceptibility of MoS_2 .

(**E**) Intensity profiles of dark-field images as a function of propagation distance x, measured on waveguides with different MoS_2 layer numbers at a single wavelength (550 nm). (**F**) Schematic illustrations of the δ -potential well with asymmetric vacuum levels V(z) and its quantum mechanical eigenstate $\psi(z)$. The oscillation is exaggerated for clarity. (**G**) Schematic of coupling of free-space laser beam into δ waveguide in asymmetric dielectric environment. (**H**) Top-view dark-field signals (λ = 750 nm) measured from monolayer MoS_2 for several $\Delta n/n_o$.

independently available for thin-film microfabrication, integration, and optical access. We can use these properties to demonstrate two approaches of optical functionalization on a δ waveguide—integration of thin-film elements (Fig. 3) and direct microfabrication and optical excitation of MoS₂ (Fig. 4).

Figure 3A displays a scanning electron microscope image demonstrating our capability of integrating thin-film optical components on a δ waveguide. A transparent dielectric film (1.8- μ m-thick SU-8) is fabricated through a

standard lithography process on a monolayer MoS_2 waveguide into convex and concave geometries designed for wavefront shaping of guided waves (inset; see materials and methods for detailed fabrication). Similarly, an ultrathin metal (5-nm-thick Au) is used to form slits, the most basic element for diffractive optics, as well as gratings (fig. S7). Figure 3B schematically illustrates the key ideas about how they work: Transparent dielectric SU-8 films with thickness t > w (where w is the mode width) can alter the effective refractive index (top) and

therefore control the wavefront of guided modes; metallic films, which have a large extinction coefficient, can carry only TM modes (not allowing TE modes to propagate; fig. S8), thereby blocking the TE-guided modes in the δ waveguide (bottom). Our simulations confirm that the effective mode index $(n_{\rm eff})$ changes from n_0 to $n_{\rm d}$ across the dielectric interface with negligible back scattering as a result of the similar mode widths $(\Delta w/w = 0.02;$ Fig. 3C, top). The simulation also shows that 5-nm-thick Au (yellow dashed line in the bottom of Fig. 3C)

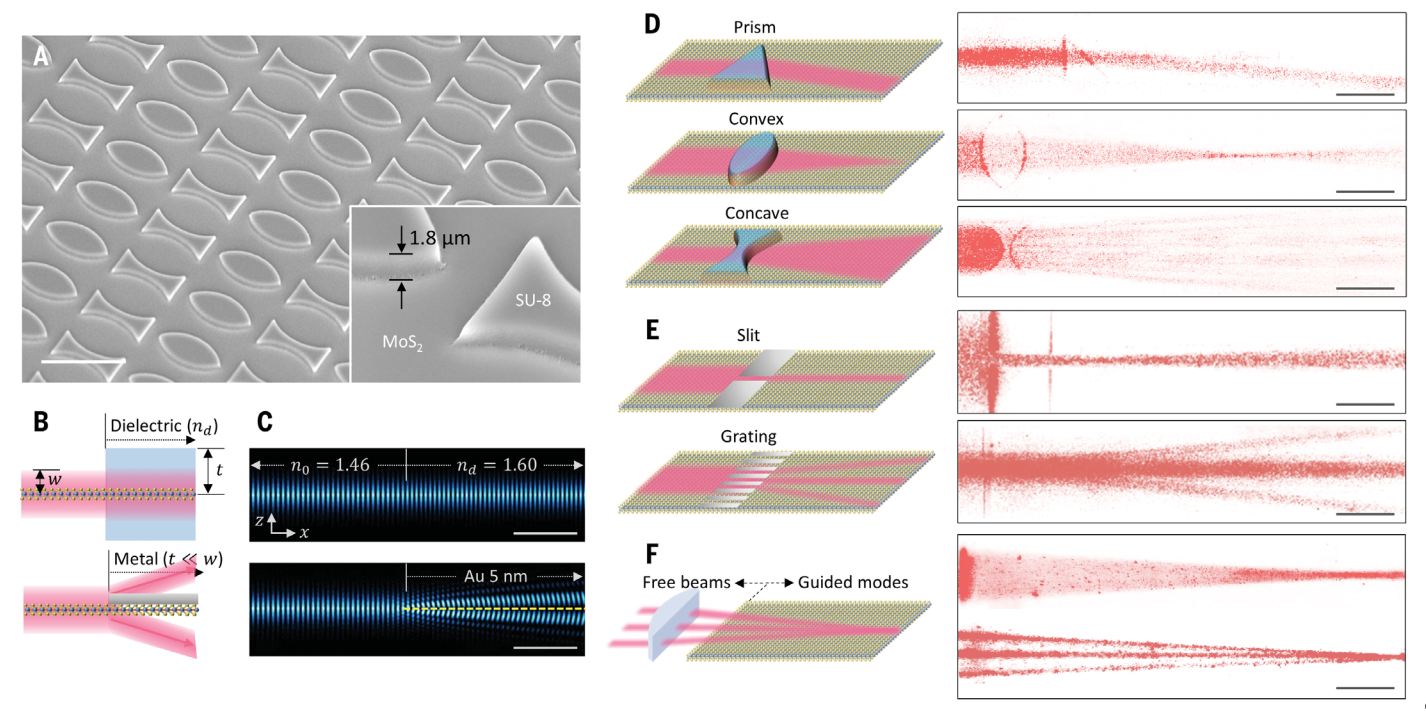


Fig. 3. Microfabricated thin-film components on δ waveguides. (A) Scanning electron microscope images of convex- and concave-shaped optical elements made of 1.8-μm-thick SU-8 film integrated on a monolayer MoS $_2$ film. Inset shows a magnified image. Scale bar, 20 μm. (B) Schematic illustration of effective index modulation of guided modes by using a thin film (top) and scattering of guided mode using a metallic film (bottom). (C) Simulated electric field intensity when a guided mode propagates and encounters an interface between different refractive indices of surrounding environment (top) and an interface between δ waveguides with a 5-nm-thick Au film and without the Au film

(bottom). Scale bars, 2 μ m. (**D**) Schematics on how guided waves interact with dielectric thin-film components microfabricated into prism, convex, and concave shapes (left) and corresponding experimental dark-field images measured in the top-view configuration (right) (λ = 720 nm). Scale bars, 0.2 mm. (**E**) Schematics of using metallic films as a slit or a grating (left) and corresponding experimental images (right). Scale bars, 0.5 mm. (**F**) Schematic of delivering a designed wavefront of 2D free beams into the guided waves (left) and corresponding experimental images (right). Scale bar, 1 mm.

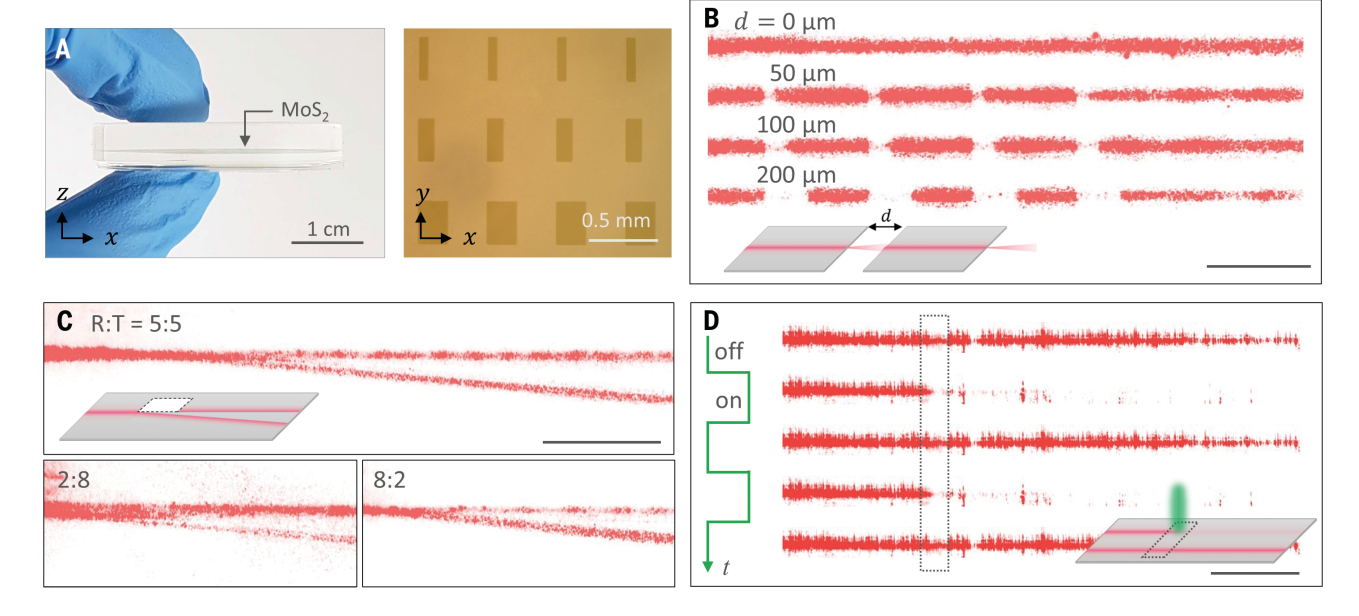


Fig. 4. Patterned and photo-modulated δ **waveguides.** (**A**) Cross-sectional photograph of a δ waveguide inside optically homogeneous polymer packaging (left) and an optical micrograph of patterned waveguides (right), generated by removing MoS₂ with a pulsed laser. (**B**) Dark-field images that demonstrate the transport of guided waves across interconnected waveguides (λ = 750 nm), where multiple waveguides are separated by a distance *d* (disconnected area

in schematic). Scale bar, 0.5 mm. (**C**) Splitting and deflecting of guided waves (λ = 750 nm), where a square area of MoS₂ is removed (dotted area in schematic). Scale bar, 1 mm. (**D**) Modulation of guided waves (λ = 680 nm), actively switchable by using a pump beam (λ = 532 nm, intensity ~ 2 kW/cm²) that is directed at a local area of MoS₂ (dotted box in schematic). Scale bar, 0.5 mm.

Lee et al., Science 381, 648-653 (2023) 11 August 2023 4 of 6

on monolayer ${\rm MoS}_2$ fully scatters the incoming waves and completely blocks the propagation of guided waves.

Figure 3, D and E, displays experimental images showing how guided waves interact with different optical elements (right; $\lambda = 720 \text{ nm}$) and corresponding schematics (left). The measured beam trajectories shown in Fig. 3D demonstrate that the refractive components change the propagation direction (by prism; top) and shape the wavefront of incident waves from planar to either convergent (by convex; middle) or divergent (by concave; bottom) forms. Placing optical elements only on top of a waveguide induces asymmetry, weakening the confinement and increasing the loss. Using symmetric refractive elements by transferring identical components on either side of MoS2 improves the transmission by up to 85% (fig. S9). The top-view images in Fig. 3E show that the ultrathin metals clearly stop the propagation of guided waves, which allows their combinations to work for diffractive optics: (i) The slit geometry (top), made by two metal sheets with a gap space (3 µm), cuts the incident beam width to leave a narrow line matching with the gap size, and (ii) the diffraction grating (bottom), an arrangement of multiple slits of the same gap space with periodicity of 5 μ m (Λ), generates the firstorder diffracted beams deflecting at 5.6 degrees, which agrees with the phase-matching condition $(\lambda/n_0\Lambda)$.

These results indicate that our approach for guided-wave optics on δ waveguides is conceptually similar to free-beam optics on an optics table. Because the guided wave is a 2D light wave with $k \approx k_{\parallel}$, the dispersion relation of the wave is practically identical to those in free space. This makes δ waveguides a unique platform that can take advantage of the near-zero structural dispersion along the trapping dimension. Figure 3F demonstrates this structural dispersion-free property, where a cylindrical convex lens is placed before the waveguide to focus one (upper image) or more (lower image) incoming laser beams in the x-y plane. The darkfield images show that the δ waveguide takes different incoming waves and makes sharp focuses within the waveguide regardless of the beam diameter and the number of incident beams. Our analysis further confirms that the wavefront designed for the 2D free beams is accurately transmitted into the guided waves, with the focal positions closely aligning with the predicted location based on the displacement of the cylindrical lens (fig. S10A). This demonstrates that δ waveguides allow impedance matching with free-space optics, and thus the 2D waveform remains during the transformation between free beams and guided modes.

In addition to guided wave optics based on thin-film integration, the MoS₂ monolayer can be patterned (Fig. 4A) or optically excited, which enables local control of the trapping

potential. We demonstrate three basic functionalities for 2D photonics: interconnection, beam splitting, and modulation. Figure 4B shows how a guided wave propagates across the interconnection geometry where a δ waveguide is disconnected into several segments separated by regions void of MoS2 with a varying gap distance d (materials and methods). The darkfield intensity suggests an excellent interconnection efficiency (~0.1-dB loss per 10-µm gap distance; fig. S10B), which is consistent with observations taken in the end-face microscopy (fig. S11) and agrees with the 2D nature of the guided wave and its free beam-like propagation. Figure 4C shows an example of how to split and divert a guided wave. For this, a square area of monolayer MoS2 in the middle of the waveguide is removed by etching the material away using a pulsed laser (dotted line). When a guided wave is directed at a corner of the square, it divides into two-one continuing along the original direction and the second one along a different path. The deflection angle (up to ~10°) and splitting ratio (8:2, 5:5, or 2:8 shown in Fig. 4C) can be controlled by the position and relative angle of the missing MoS₂ square. This splitting behavior only occurs when a combination of a corner and tilted edges is placed in the guided beam path. It is not seen in other simpler configurations or when a corner is introduced to a decoupled beam (fig. S12). Fig. 4D presents an active switching of the guided wave transport. A pump beam (532 nm; intensity $I_P \sim 2 \text{ kW/cm}^2$) is introduced normal to the MoS₂ waveguide that intersects with the guided wave (dotted area; see materials and methods). The 2D wave strongly attenuates when the pump beam is on and fully recovers its original intensity when the pump beam is off. This shows that the transport of a guided wave can be modulated using a pump beam absorbed by MoS₂. The efficiency of the photo-modulation increases monotonically with I_P reaching 50% at 0.5 kW/cm², which suggests that the photo-modulation occurs in the linear absorption regime for MoS₂ (fig. S13). Although many of these observations can be explained by polariton-exciton interactions (30), more theoretical and experimental studies will be needed to fully understand these phenomena.

Conclusions

Our approach of producing δ waveguides can be extended to other atomically thin materials and heterostructures for the development of ultrathin integrated photonic circuits as well as to explore the specific properties of light waves guided by 2D materials. For example, light waves with widely different wavelengths (far-infrared to ultraviolet) can be guided by a single δ waveguide, enabling multioctave-spanning photonic architectures. The broadband, high-power, and dispersion-free operation of our δ waveguides could be used for 2D non-

linear photonics capable of on-chip manipulation of pulsed signals and highly efficient second-harmonic generator when combined with nonlinear properties of vdW materials. The extensive library of light-matter interactions in atomically thin materials could allow for the integration of advanced photonic devices with a δ waveguide, where multiple components with advanced plasmonic and excitonic properties can be deposited and patterned at large scale using conventional thin-film processes.

REFERENCES AND NOTES

- 1. L. Feng et al., Science 333, 729-733 (2011).
- A. Politi, M. J. Cryan, J. G. Rarity, S. Yu, J. L. O'Brien, Science 320, 646–649 (2008).
- Q. Xu, B. Schmidt, S. Pradhan, M. Lipson, *Nature* 435, 325–327 (2005).
- H. Rong et al., Nature 433, 725–728 (2005).
- H. Hodaei, M. A. Miri, M. Heinrich, D. N. Christodoulides, M. Khajavikhan, Science 346, 975–978 (2014).
- M. Lee, S. Callard, C. Seassal, H. Jeon, Nat. Photonics 13, 445–448 (2019).
- A. W. Elshaari, W. Pernice, K. Srinivasan, O. Benson, V. Zwiller, Nat. Photonics 14, 285–298 (2020).
- 8. G. Crosnier et al., Nat. Photonics 11, 297-300 (2017).
- 9. T. Harter et al., Nat. Photonics 12, 625-633 (2018).
- J. Wang, F. Sciarrino, A. Laing, M. G. Thompson, *Nat. Photonics* 14, 273–284 (2020).
- 11. K. Y. Yang et al., Nat. Photonics 12, 297-302 (2018).
- 12. J. B. Khurgin, Optica 2, 740-742 (2015).
- 13. J. Chen et al., Nature 487, 77-81 (2012).
- 14. G. X. Ni et al., Nature 557, 530-533 (2018).
- D. N. Basov, M. M. Fogler, F. J. García de Abajo, Science 354, aag1992 (2016).
- 16. T. Low et al., Nat. Mater. 16, 182-194 (2017).
- 17. E. Yoxall et al., Nat. Photonics 9, 674-678 (2015).
- 18. Q. Zhang et al., Nature 597, 187-195 (2021).
- 19. L. Xiong et al., Sci. Adv. 7, eabe8087 (2021).
- 20. Y. Zhou et al., Nat. Nanotechnol. 12, 856–860 (2017).
- 21. F. Hu et al., Nat. Photonics 11, 356-360 (2017).
- 22. F. Hu et al., Phys. Rev. B 100, 121301 (2019).
- 23. X. Zhang et al., Nat. Nanotechnol. 14, 844-850 (2019).
- 24. F. Barachati et al., Nat. Nanotechnol. 13, 906-909 (2018).
- M. Mrejen, L. Yadgarov, A. Levanon, H. Suchowski, Sci. Adv. 5, eaat9618 (2019).
- 26. Y. Li et al., Phys. Rev. B 90, 205422 (2014).
- 27. K. Kang et al., Nature **520**, 656–660 (2015).
- 28. K. Kang et al., Nature 550, 229-233 (2017).
- 29. A. M. van der Zande *et al.*, *Nat. Mater.* **12**, 554–561 (2013).
- 30. P. Cristofolini *et al.*, *Phys. Rev. Lett.* **110**, 186403 (2013).
- M. Lee et al., Data and codes for: "Wafer-scale δ-waveguides for integrated two-dimensional photonics," Zenodo (2023); https://doi.org/10.5281/zenodo.8080270.

ACKNOWLEDGMENTS

We thank B. Cheng, P. Poddar, and T. Zhong for their helpful discussions. Funding: Primary funding for this work comes from the Air Force Office of Scientific Research (FA9550-21-1-0323 and FA9550-16-1-0347) and the MURI project (FA9550-18-1-0480). Additional funding was provided by the University of Chicago MRSEC (NSF DMR-2011854) and the Cornell Center for Materials Research (NSF DMR-1719875). F.M. acknowledges support by the NSF Graduate Research Fellowship Program under grant no. DGE 1746045, A.Y. is supported by the Department of Defense through the National Defense Science and Engineering Graduate (NDSEG) Fellowship Program. This work made use of the characterization facilities of the University of Chicago MRSEC (NSF DMR-2011854) and the fabrication facilities of the Pritzker Nanofabrication Facility at the University of Chicago, which receives support from SHyNE Resource (NSF ECCS-420 1542205), a node of NSF's NNCI network Author contributions: MI HH and IP conceived the experiments. M.L. and H.H. fabricated the devices, conducted optical measurements, and performed electrodynamics simulations. J.Y. performed the laser patterning. F.M. and C.L. synthesized monolayer MoS2 films. M.L., H.H., and A.Y. developed the polymer and liquid encapsulation processes for index matching, H.H. developed the thin-film element integration

Lee et al., Science 381, 648-653 (2023) 11 August 2023 5 of 6

process. M.L., H.H., and J.P. wrote the manuscript. All authors discussed and commented on the manuscript. **Competing interests**: The authors declare no competing interests. **Data and materials availability:** All data are reported in the main text and supplementary materials. Raw data and relevant codes can be found at Zenodo (31). **License information**: Copyright © 2023 the authors, some rights reserved; exclusive licensee American

Association for the Advancement of Science. No claim to original US government works. https://www.science.org/about/science-licenses-journal-article-reuse

SUPPLEMENTARY MATERIALS

science.org/doi/10.1126/science.adi2322 Materials and Methods Supplementary Text Figs. S1 to S15 Table S1 References (32–34)

Submitted 12 April 2023; accepted 30 June 2023 10.1126/science.adi2322

Lee et al., Science 381, 648-653 (2023) 11 August 2023 6 of 6